Journal of Molecular Catalysis A: Chemical 323 (2010) 78–83

Contents lists available at ScienceDirect

Journal of Molecular Catalysis A: Chemical

journal homepage: www.elsevier.com/locate/molcata

Synthesis, characterization, and antimicrobial application of nano-palladium-doped nano-WO_3

M.A. Gondal[a,*], A. Bagabas[b], A. Dastageer[a], A. Khalil[a]

[a] Laser Research Group, Physics Department and Center of Excellence in Nanotechnology, King Fahd University of Petroleum & Minerals, Dhahran 31261, Saudi Arabia
[b] Petrochemicals and Refining Center, Petroleum and Petrochemicals Research Institute (PAPRI), King Abdulaziz City for Science and Technology (KACST), P.O. Box 6086, Riyadh 11442, Saudi Arabia

ARTICLE INFO

Article history:
Received 4 February 2010
Received in revised form 6 March 2010
Accepted 15 March 2010
Available online 20 March 2010

Keywords:
Nano-palladium-doped nano-tungsten trioxide
Near resonance photocatalysis
Laser-induced photocatalysis
Escherichia coli

ABSTRACT

Nano-tungsten trioxide (n-WO_3) was synthesized by dehydrating tungstic acid (H_2WO_4) at 300 °C. Nano-palladium (n-Pd) was then loaded as 10 wt% on this n-WO_3 by impregnation for the synthesis of the desired n-Pd/n-WO_3 photocatalyst. This loading process enhanced the photocatalytic activity of n-WO_3 for the removal of *Escherichia coli* microorganism from water when applying 355-nm UV laser radiation. The absorption and photoluminescence spectra revealed a blue-shift for the band gap energy (E_g) from 2.71 eV for the undoped n-WO_3 to 3.5 eV for the doped one. This shift in E_g caused a near resonance condition, which accounts for the significant improvement of the photocatalytic activity upon doping n-WO_3.

1. Introduction

Palladium (Pd)-doped metal oxide semiconductors exceed their corresponding undoped ones in the photocatalytic [1–3] and gas sensing applications [4,5]. For instance, Pd-doped catalysts exhibit superior activity for hydrogen production through water splitting [6–9], conversion of methane into methanol [10,11], removal of phenol and dyes from wastewater [12–14]. This improvement in photocatalytic performance is partially due to alteration of the semiconductor's band gap energy upon doping in accordance to Moss–Burstein effect, which is based on the Pauli Exclusion Principle [15–17]. Furthermore, enhancement of semiconductor's photocatalytic performance can be achieved upon reduction of its particle size to the nano-scale [18]. The particle nanosize results in a quantum confinement for the exciton within the particle and in widening of its E_g. Such nanosize enhancement was responsible for the 45% higher antimicrobial activity of the undoped n-WO_3, synthesized in our laboratory, in the process of disinfection of water, contaminated with *Escherichia coli*, when compared to that of the undoped commercially available micron-sized tungsten trioxide (μ-WO_3) [19].

In the present work, we combined the doping and nanosize effects for further enhancement of the photocatalytic performance. This goal was accomplished by synthesizing and characterizing 10 wt% n-Pd loaded n-WO_3 (n-Pd/n-WO_3). This photocatalyst was used in the disinfection process of *E. coli* microorganism in water while applying 355-nm UV laser radiation. The effect of n-Pd/n-WO_3 on the bacterial decay process was also investigated in terms of bacterial decay curves with different pulse energies of 355 nm laser radiation and different concentrations of photocatalyst.

2. Experimental

2.1. Materials

Tungstic acid (>99%, Fluka), palladium acetate (99.98%, Aldrich) and benzene (thiophene-free, Fisher Scientific) were commercially available and were used as received without further purification.

2.2. Physical and analytical measurements

UV–vis absorption spectra were recorded from 190 to 800 nm on a spectrophotometer (Jasco model 570). The PL spectra were recorded in the range of 300–800 nm on a spectro-fluorometer (Shimadzu model RF-5301 PC with 1200 grooves/mm). The surface chemical composition of the photocatalysts were determined by X-ray photoelectron spectroscopy (XPS). The XPS spectrometer used in this work is VG Scientific (Model ESCA Lab MK2), the operating voltage of XPS is 13 kV and X-ray source is Al K line (1486.6 eV). The morphology and particle size and shape of n-Pd/n-WO_3 were exam-

* Corresponding author. Tel.: +966 38602351; fax: +966 38602293.
E-mail address: magondal@kfupm.edu.sa (M.A. Gondal).

1381-1169/$ – see front matter © 2010 Elsevier B.V. All rights reserved.
doi:10.1016/j.molcata.2010.03.019

ined by high resolution transmission electron microscope (model: JEM-2100F (HR)) at a voltage of 200 kV. A sample of this material was suspended in acetone by ultra-sonication. A drop of this suspension was then mounted on a carbon-coated copper grid for analysis.

2.3. Catalyst preparation

Undoped *n*-WO_3 was synthesized from tungstic acid (H_2WO_4) by dehydration. *n*-WO_3·*n*-Pd metal was loaded on the prepared *n*-WO_3 by impregnation method using palladium acetate [$Pd(OAc)_2$] as a source for *n*-Pd. The required amount of $Pd(OAc)_2$, to give 10 wt% *n*-Pd loading, was mixed and was pulverized with the *n*-WO_3. Anhydrous, sulfur-free benzene of about 20 ml was added to the mixture of $Pd(OAc)_2$ and *n*-WO_3. This mixture was mechanically stirred to ensure the homogeneous distribution of $Pd(OAc)_2$ over the *n*-WO_3 support. After stirring step, benzene was evaporated under vacuum using rotary evaporator. Dissolving of $Pd(OAc)_2$ and evaporating of benzene were performed three times to guarantee the homogeneous distribution of $Pd(OAc)_2$. After the third evaporation process, the left solid was ground and was heated for 5 h in a programmable, tubular furnace under a flow of 50 ml/min of highly pure hydrogen (H_2, 99.999%), at 350 °C, for the reduction of $Pd(OAc)_2$ to *n*-Pd metal.

Palladium acetate was reduced to palladium metal to enhance the photocatalytic activity of tungsten trioxide via the prevention of exciton recombination and increase the efficiency of charge separation. Generally speaking, noble metals such as gold, platinum, and palladium are loaded on the semiconductor surface for such purpose. For instance, many investigators have demonstrated that the photocatalytic activity may be enhanced by impregnating the surface of TiO_2 with noble metals [20–22]. Similar approach has been adopted to increase the catalytic activity of TiO_2 by depositing metals as heterojunction. In addition, metal (Pt, Au, or Pd)-doped semiconductor system was prepared to investigate the effect of both physical and chemical characteristics of the catalyst together with their influence on the photocatalytic activity of TiO_2 towards the photocatalytic degradation of acid green [22]. Sakthivela and his coworkers [23] also studied the enhancement of the photocatalytic activity by reducing the deposited metal before testing the photocatalytic activity. Carrying out the reaction in water would not oxidize the noble metal, palladium, because it possesses a relatively high, positive standard reduction potential of 0.987 V [24]. After reduction process, the sample was kept under hydrogen in a desiccators until it was used.

2.4. Photocatalytic reaction

A 355-nm wavelength high power laser beam, generated from the third harmonic of the Spectra Physics Nd:YAG laser (Model GCR 250), with a pulse width of ~8 ns, was used as a radiation source. During this study, laser energy, amount of catalyst (particle density), stirring rate, and laser beam diameter were found to affect significantly the reaction rate (removal of bacteria). The latter two parameters were kept constant for all the studies, reported in this paper. However, the dependence of bacteria removal on laser energy, amount of catalyst and laser irradiation time was carefully optimized for the maximum disinfection of water. The destructive effect of focused laser beam was minimized by expanding the diameter of the beam to 1 cm by using a set of lenses and mirrors. The water samples, contaminated with bacteria, were irradiated using Nd:YAG laser, at different incident laser energies, amounts of catalyst (undoped and doped WO_3) and for different times. In order to investigate the effect of incident laser energy on removal of microorganism, different laser energies were applied. In each case, the amount of catalyst was kept constant and the samples were collected after the exposure at a specific time interval.

2.5. Bacteria culturization and growth

Nutrient broth medium was prepared by dissolving 8 g of nutrient broth in 1000 ml of distilled water (pH adjusted to 7.5) and sterilized at 121 °C at 2 bar pressure for 30 min. *E. coli* K12 wild-type strain (MG 1655) were grown overnight in nutrient broth at 37 °C on a rotary shaker (160 rpm). Aliquots of the broth medium containing *E. coli* were inoculated into fresh broth medium and incubated in the same conditions. Then, *E. coli* cells were harvested from the broth culture by centrifugation at 4000 × *g* for 10 min at 4 °C, washing twice with a sterile 0.9% NaCl solution at 4 °C and divided into two groups: test and control. In the test group *E. coli* cells were suspended in the photocatalytic solution to a concentration of 2×10^7 colony forming units per milliliter (CFU/ml). In the control group *E. co*li cells were suspended in the same concentration in the normal saline.

The nutrient agar plates were prepared by the addition of 15 g of agar to the nutrient broth medium, sterilized as above, poured into Petri dishes and left to cool down and solidify at room temperature. Aliquots from both groups of *E. coli* (the test and control) were serially diluted with normal saline and aliquots from each dilution inoculated separately on the nutrient agar plates and incubated at 37 °C. Colonies of the both groups were counted after 48 h and compared with each other.

3. Results and discussion

The undoped and doped *n*-WO_3 photocatalysts were characterized by X-ray photoelectron spectroscopy (XPS) for both pure nano-WO_3. We identified the peaks using the characteristic binding energies of different levels of the elements available in the data base incorporated in the analysis software. Tungsten, oxygen and palladium peaks are identified in Fig. 1a for the *n*-Pd/*n*-WO_3. On the other hand, Fig. 1 b displays tungsten and oxygen peaks for the undoped *n*-WO_3. The small carbon peak (C 1s) in these XP spectra at 285 eV is due to the carbon paste, used to stick the sample on the mount. Considering the purity of the material we used, and the fact that the carbon paste was used to hold the sample, we attribute the C 1s peak originating from the paste. The X-ray powder diffraction, XRD (not shown) study on the *n*-Pd/*n*-WO_3 revealed that the average crystallite size of WO_3 was 14 nm, using Scherrer's equation by averaging results from the three main crystallographic directions [25].

Our earlier work [18] showed an enormous effect on the photocatalytic process using *n*-WO_3 due to quantum confinement, and its consequent widening of the E_g from 2.61 eV for μ-WO_3 to 2.71 eV for *n*-WO_3. Accordingly, to understand the effect of doping *n*-WO_3 with *n*-Pd on the E_g, the absorption and photoluminescence spectra were recorded for the *n*-Pd/*n*-WO_3 photocatalyst. Fig. 2 depicts the absorption spectra of the undoped *n*-WO_3 (Fig. 2a) and the *n*-Pd/*n*-WO_3 (Fig. 2b). For both spectra, the *x*-axis is the energy (E) in eV and *y*-axis is the square of the product of absorbance and energy $(a \times E)^2$. Such plot usually gives a straight line curve in the case of direct band gap material. The extrapolation of the linear part of the curve to the energy-axis gives the E_g of the semiconductor material. From Fig. 2, it is estimated that the E_g of the undoped *n*-WO_3 is around 2.71 eV and that for the *n*-Pd/*n*-WO_3 is 3.5 eV. In order to confirm such a huge increase in the band gap energy upon doping, we recorded the room-temperature photoluminescence (PL) spectra of both undoped *n*-WO_3 (Fig. 3a) and doped (Fig. 3b) by using 300-nm excitation wavelength. The maximum PL wavelength for the doped one is 366 nm (3.5 eV) and that for the undoped one is

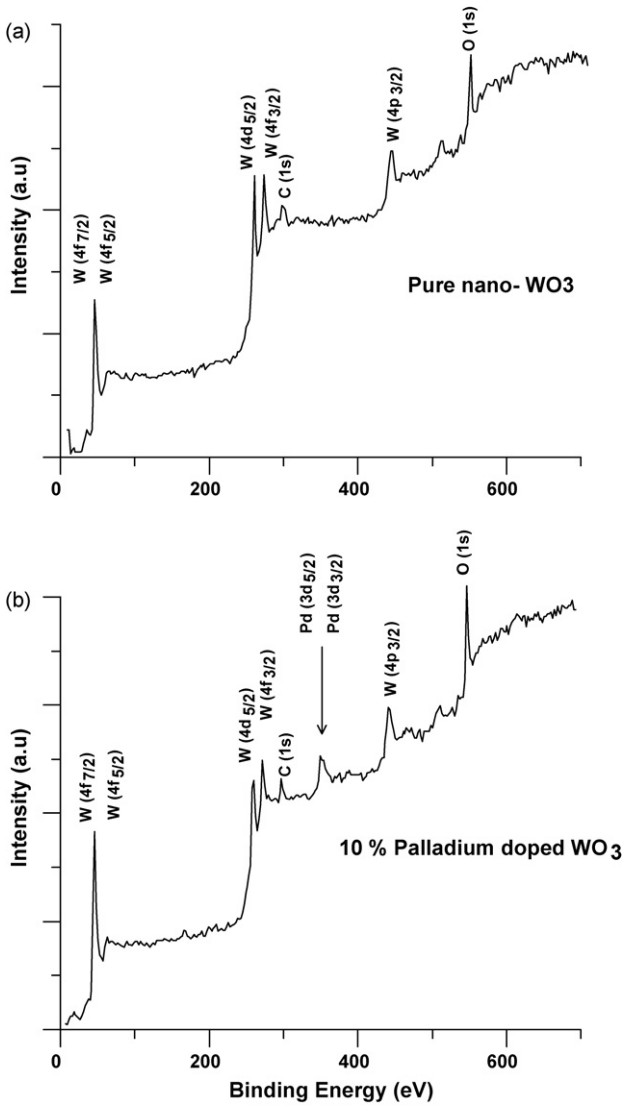

Fig. 1. X-ray photoelectron spectra of (a) undoped n-WO_3 and (b) n-Pd/n-WO_3. The elements are identified on the figure.

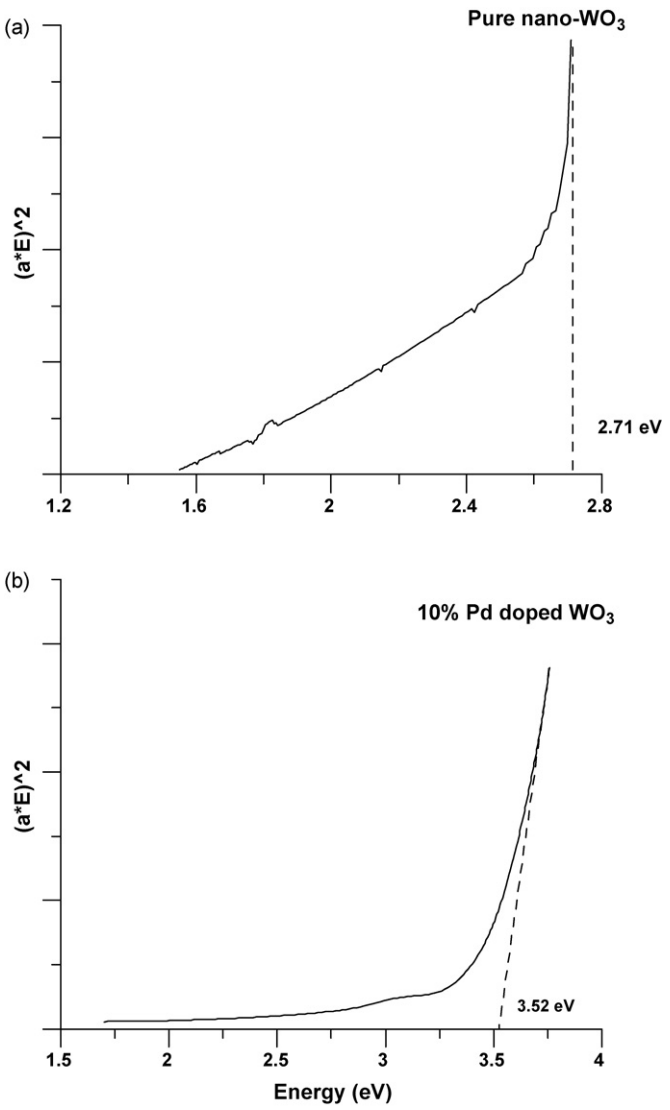

Fig. 2. Absorption spectra of (a) undoped n-WO_3 and (b) n-Pd/n-WO_3. The band gap energies are marked.

458 nm (2.71 eV). The two different optical studies consistently and precisely give the same % increase in the band gap energy (10%) for n-Pd/n-WO_3, as compared to the undoped n-WO_3.

The widening of the E_g upon doping is due to Moss–Burstein effect, resulting from Pauli Exclusion Principle [15–17]. The energy difference between the highest level of the valance band (VB) and the lowest level of the conduction band (CB) is the E_g. When the semiconductor is doped, the Fermi energy level (E_f) lies within the CB by certain energy (E_n). Since the states below the energy E_n are already filled, the fundamental transitions to states below $E_g + E_n$ are forbidden. Hence, the absorption edge should shift to higher energies by about E_n, and consequently the measured E_g is determined from the onset of inter-band absorption and moves to higher energy or blue shifted. The blue shifting of the E_g has an enormous impact on the photocatalytic activity of the material. In photocatalysis, the catalytic material becomes more effective when there is some sort of resistance that blocks the electron hole recombination. Upon excitation, the electron jumps to the CB leaving a positively charged hole in the VB. In an effective photocatalyst, more electrons in the CB are used for the catalytic activity rather than letting them recombine with the holes in the VB. In our case, due to the extra energy E_n by which the E_f is embedded into the conduction band, it somehow inhibits the recombination process and makes the electrons available for effective photocatalysis.

Morphology investigation of the synthesized n-Pd/n-WO_3 by TEM revealed that the n-WO_3 support adopts random shapes in a size range of 60–120 nm (Fig. 4a). On the other hand, the n-Pd particles adopt almost spherical shape while their size falls in the range of 4–10 nm (Fig. 4a and b). Furthermore, they are highly dispersed on the surface of the n-WO_3 support (Fig. 4a). Such observation can be accounted for increasing the photocatalytic activity of n-Pd/n-WO_3, because the high dispersion provides high surface area contact for reaction, an essential feature for high catalytic activity. Fig. 4b provides a high resolution image where the lattice plane fringes of both the n-Pd and n-WO_3 can be observed and distinguished from each other. Both images in Fig. 4 clearly show that the n-Pd particles reside on the surface of the n-WO_3 support. This residual may contribute to the enhancement of electron–hole separation on the surface of n-WO_3 support.

The enhancement of the photocatalytic activity due to the doping of n-WO_3 was investigated for the disinfection of *E. coli* microorganism in water and the result was compared to that of undoped n-WO_3. In addition, it has been established that the undoped n-WO_3 has higher photo catalytic activity than the n-

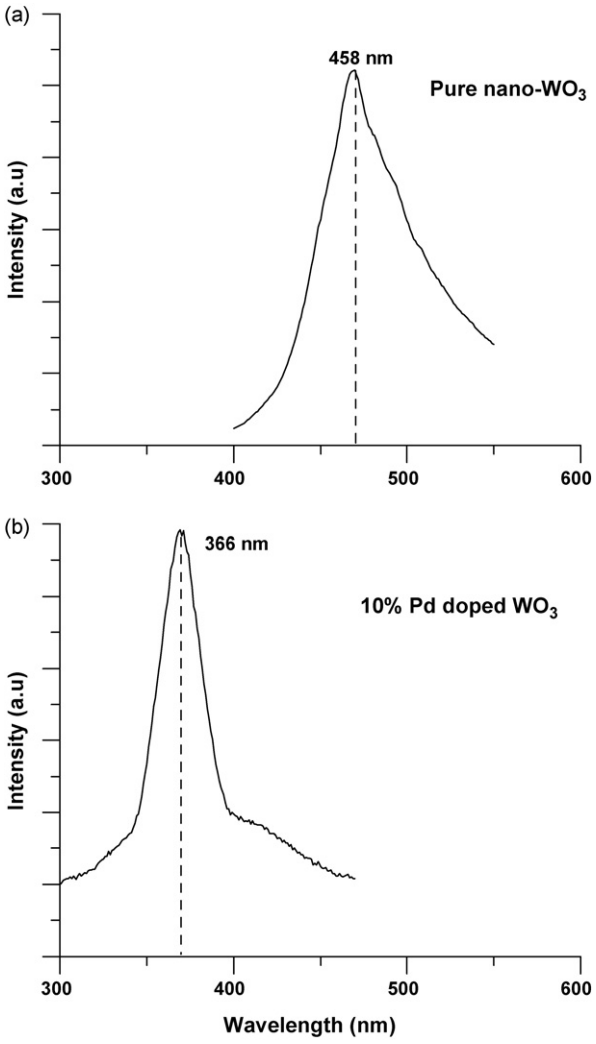

Fig. 3. Photoluminescence (PL) spectra of (a) undoped nano-WO_3 and (b) *n*-Pd/*n*-WO_3.

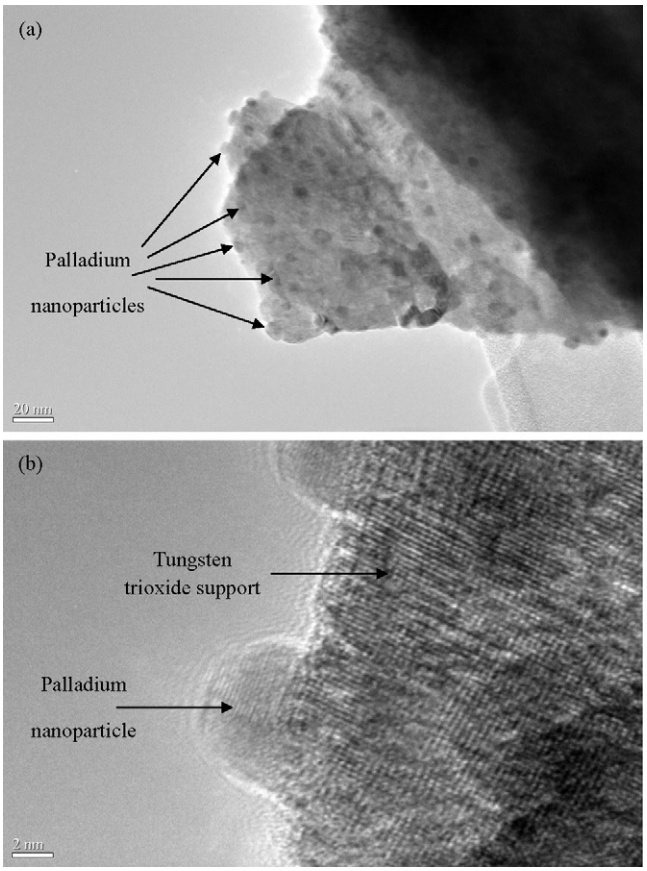

Fig. 4. TEM electron micrographs of *n*-Pd/*n*-WO_3 (a) at magnification of 80k and (b) high resolution at magnification of 800k.

WO_3 [18]. Fig. 5 shows the bacteria decay curves when the undoped *n*-WO_3 and the doped one (*n*-Pd/*n*-WO_3) were used as a photocatalyst. The growth and decay of the bacterial population are typically exponential in nature, and hence, we quantify the bacterial decay process as the rate constant that appears in the exponential function. All the decay curves in this work are presented as a natural logarithm (ln) of N/N_0 versus the irradiation time. N_0 is the initial normalized population, which we maintained a constant value of 4×10^7 CFU/ml. *N* is the diminishing number of bacterial population in the unit of CFU/ml. From the decay curve, we directly estimated the decay constant from the slope. For Fig. 5a, the *n*-WO_3 concentration is 3.75 mg/ml and the laser pulse energy is 100 mJ, while for Fig. 5b, the concentration of *n*-Pd/*n*-WO_3 is only 1 mg/ml and the laser pulse energy is also reduced to 80 mJ. This reduction in concentration and the laser pulse energy is in order to have some measurable decay curve; else the curve will be too steep to record. The decay curves presented in Fig. 5 is just to give a qualitative comparison between doped and undoped WO_3, and intended for quantitative aspect. Although the laser pulse energy and the concentration of the catalyst is weaker in the case of *n*-Pd/*n*-WO_3, the decay constant estimated from Fig. 5a and b has shown a significant increase. For *n*-Pd/*n*-WO_3, the decay constant is about 1.1 min^{-1} and for the undoped *n*-WO_3 is about 0.94 min^{-1}. However, the threshold time in both cases is almost instant.

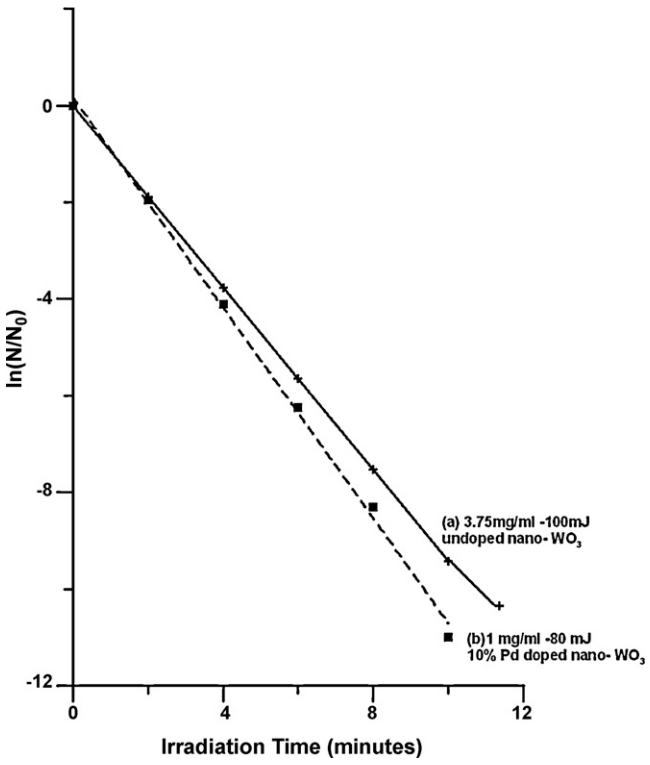

Fig. 5. Comparison of bacterial decay curve as natural log of N/N_0 versus the light exposure time for (a) undoped *n*-WO_3 of catalyst concentration of 3.75 mg/ml and 100 mJ laser pulse energy and (b) *n*-Pd/*n*-WO_3 1 mg/ml and 80 mJ laser pulse energy.

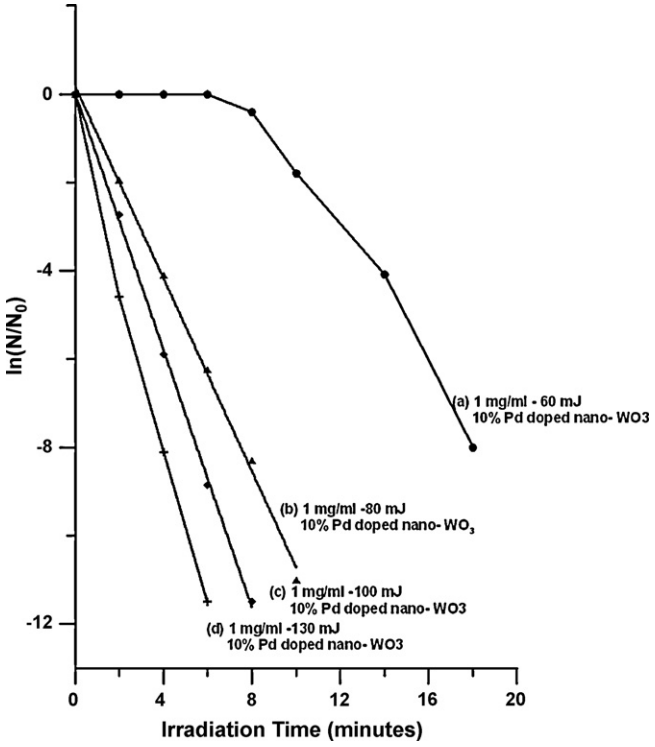

Fig. 6. Bacterial decay curve as natural log of N_0/N versus the light exposure time *n*-Pd/*n*-WO_3 with different laser pulse energies (a) 60 mJ/pulse, (b) 80 mJ/pulse and (c) 100 mJ/pulse laser irradiation at 355 nm. The catalyst concentration was 1 mg/ml.

The two important parameters that affect the bacterial decay process are the catalyst concentration and laser pulse energy. In Fig. 5, we compare the bacterial decay curves due to two different photocatalysts (n-WO_3- and Pd-doped n-WO_3). Technically these are the two different photocatalyst with completely different catalytic behavior and hence Fig. 5 depicts only the relative merit of Pd doping by indicating an enhancement of decay process, although the laser pulse energy and catalyst concentration is less than that in the non-doped case. The process of bacterial disinfection is due to the creation of highly oxidizing radicals that oxidize the cell membrane of the microorganism and damage them [26–28]. With the increased band gap after doping with palladium, the electron–hole recombination process gets slowed down and more electrons are used for the creation of the oxidizing radicals.

Fig. 6 shows the bacterial decay curves for different laser pulse energies. For all the curves, the starting population is 10^7 CFU/ml and the minimum detection of bacteria is set to be approximately 100 CFU/ml. This corresponds to a minimum of $\ln(N/N_0) = -11.5$, and hence, we can not present a *y*-axis value less than −11.5, which in our case, corresponds to 0 CFU/ml. The bacterial decay curve can be characterized by three factors: decay constant, threshed time for decay process, and the time required for the complete depletion. In an ideal disinfection process, the decay rate constant should be high, the decay threshold time should be zero (instant) and the depletion time should be as short as possible. Of course, these three factors mainly depend on the nature and the concentration of catalyst and the laser pulse energy. For the decay curves in Fig. 6(b)–(d), the onset time is almost zero (instant) due to the higher laser pulse energy but in the case of Fig. 6(a), a plateau appears in the decay curve due to the longer threshold time as a result of lower pulse energy. Also, more incident laser energy means more photons available for active sites on the catalyst surface which enhances the disinfection process. Hence at lower incident laser energy, less active sites are possible so the reaction process is slow and takes quite to while to build up. This is the reason why we see plateau at the lower pulse energy decay curve.

The slope of the bacterial decay curve (Fig. 6) increases with the increase of laser pulse energy for a constant catalyst concentration of 1 mg/ml, while the threshold time of the decay is instant except for the 1 mg/ml concentration and 60 mJ laser pulse energy (Fig. 6a). In the case of curve Fig. 6a, the threshold time is 8 min and the complete killing takes place approximately in 24 min. When increasing the laser pulse energy from 60 to 130 mJ, the decay constant increased and the time, taken for the complete killing of bacteria, decreased. In the case of Fig. 6b, where the pulse energy is 80 mJ, the decay constant is 1.1 min^{-1} and the time for complete depletion of bacteria is less than 12 min. However, increasing the pulse energy to 100 mJ, Fig. 6c resulted in increasing the decay constant to 1.45 min^{-1} and in decreasing the time for complete depletion to 8 min. Furthermore, increasing the laser pulse energy to 130 mJ led to increase the decay constant to 1.9 min^{-1} and to decrease the depletion time to less than 6 min. Although the photon energy is sufficient for transferring the electrons from the VB to the CB, the increase in the laser pulse energy allows more electrons to be available in the CB, i.e. the process resembles the usual absorption, where the transition probability depends on the radiation density.

4. Conclusions

The *n*-WO_3 was synthesized in our laboratory by dehydration process of tungstic acid (H_2WO_4) as a support for nano-palladium metal, loaded by impregnation method. The new *n*-Pd/*n*-WO_3 showed a substantial increase in the band gap energy, as reflected by the absorption and photoluminescence spectra, which consistently and precisely provided a blue shift in the E_g from 2.71 eV for *n*-WO_3 to 3.5 eV for *n*-Pd/*n*-WO_3. This new band gap energy of 3.5 eV (366 nm) of *n*-Pd/*n*-WO_3 is in near resonance with the wavelength of the excitation source (355 nm). This near resonance condition, in conjunction with the widened band gap energy significantly improves the photocatalytic activity in the disinfection of the *E. coli* microorganism from water as compared to the undoped nano-WO_3 as a photocatalyst. Furthermore, the high dispersity of *n*-Pd particles on the surface of the *n*-WO_3 support, as observed by TEM, may play a key role in the enhancement of the photocatalytic activity.

Acknowledgements

The support by King Abdulaziz City for Science and Technology (KACST) through project number 28-40 and King Fahd University of Petroleum & Minerals (KFUPM) is gratefully acknowledged.

References

[1] M.A. Aramendia, V. Borau, J.C. Colmenares, Appl. Catal. B 80 (2008) 88–97.
[2] T. Seki, J.D. Grunwaldt, N. Van, A. Vegten, Baike, Adv. Synth. Catal. 350 (2008) 691–705.
[3] U.G. Singh, J. Li, J.W. Bennett, A.M. Rappe, R. Shashadhre, S.L. Scott, J. Catal. 249 (2007) 349–358.
[4] M.V. Vaishampayan, R.G. Deshmukh, I.S. Mulla, Sens. Actuators B 131 (2008) 665–672.
[5] C. Liewhiran, S. Phanichphant, Sensors 7 (2007) 1159–1184.
[6] H. Zeng, P. Liu, W. Cai, S. Yang, X. Xu, J. Phys. Chem. C 112 (2008) 19620–19624.
[7] A. Hameed, M.A. Gondal, J. Mol. Catal. A 233 (2005) 35–41.
[8] T. Matsunga, R. Tomoda, T. Nakajima, T. Nakajima, T. Komine, Appl. Environ. Microbiol. 54 (1988) 1330–1333.
[9] T.Y. Leung, C.Y. Chan, C. Hu, J.C. Yu, P.K. Wong, Water Res. 42 (2008) 4827–4837.
[10] A. Hameed, M.A. Gondal, Z.H. Yamani, A.H. Yahya, J. Mol. Catal. A 227 (2005) 241–247.
[11] M.A. Gondal, A. Hameed, Z.H. Yamani, J. Mol. Catal. A 222 (2004) 259–265.
[12] M.A. Gondal, M.N. Sayeed, Z. Seddighi, J. Hazard. Mater. 155 (2008) 83–89.
[13] M. Qamar, M.A. Gondal, Z.H. Yamani, Catal. Commun. 10 (2009) 1980–1984.

[14] M.A. Gondal, K. Hayat, Z.H. Yamani, K. Al-Hooshani, J. Hazard. Mater. 170 (2009) 584–589.
[15] F.K. Shan, B.I. Kim, G.X. Liu, J.Y. Shon, W.J. Lee, B.C. Shin, Y.S. Yu, J. Appl. Phys. 95 (2004) 4772–4776.
[16] E. Burstein, Phys. Rev. 93 (1954) 632–633.
[17] T.S. Moss, Proc. Phys. Soc. (Lond.) B76 (1954) 775–782.
[18] M.R. Singh, J. Phys. B 39 (2006) 5131–5142.
[19] M.A. Gondal, M.A. Dastageer, A. Khalil, Catal. Commun. 11 (2009) 214–219.
[20] M. Sadeghi, W. Liu, T.G. Zhong, P. Stavropoulos, B. Levy, J. Phys. Chem. 100 (1996) 19466–19474.
[21] S. Sakthivel, M.V. Shankar, M. Palanichamy, B. Arabindoo, V. Murugesan, J. Photochem. Photobiol. A: Chem. 148 (2002) 153–162.
[22] T. Sakata, T. Kawai, K. Hashimoto, Chem. Phys. Lett. 88 (1982) 50–54.
[23] S. Sakthivela, M.V. Shankarb, M. Palanichamyb, B. Arabindoob, D.W. Bahnemanna, V. Murugesan, Water Res. 38 (2004) 3001–3008.
[24] A. Troupis, A. Hiskia, E. Papaconstantinou, Appl. Catal. B: Environ. 52 (2004) 41–48.
[25] A. Bagabas, M. Gondal, A. Khalil, A. Dastageer, Z. Yamani, M. Ashameri, 10th International Symposium "Scientific Bases for the Preparation of Heterogeneous Catalysts", Louvain-la-Neuve, Belgium, 2010.
[26] I.W. Hamley, R.W. Kelsall, M. Geoghegan, Nanoscale Science and Technology, John Wiley & Sons, New York, 2005.
[27] M. Di Ventra, Introduction to Nanoscale Science and Technology, Springer, New York, 2004.
[28] X. Chang, J. Huanga, Q. Tana, M. Wang, G. Ji, S. Deng, G. Yu, Catal. Commun. 10 (2009) 1957–1961.